Use of Convolutional Neural Network Image Classification and High-Speed Ion Probe Data Toward Real-Time Detonation Characterization in a Water-Cooled Rotating Detonation Engine

Kristyn B. Johnson
Thermal Sciences Team,
National Energy Technology Laboratory,
Morgantown, WV 26507;
NETL Support Contractor,
Morgantown, WV 26505
e-mail: kristyn.johnson@netl.doe.gov

Donald H. Ferguson
Thermal Sciences Team,
National Energy Technology Laboratory,
Morgantown, WV 26507
e-mail: donald.ferguson@netl.doe.gov

Andrew C. Nix[1]
Department of Mechanical and
Aerospace Engineering,
West Virginia University,
Morgantown, WV 26505;
Oak Ridge Institute for Science and Education,
Oak Ridge, TN 37831
e-mail: andrew.nix@mail.wvu.edu

As rotating detonation engines (RDEs) progress in maturity, the importance of monitoring advancements toward development of active control becomes more critical. Experimental RDE data processing at time scales which satisfy real-time diagnostics will likely require the use of machine learning. This study aims to develop and deploy a novel real-time monitoring technique capable of determining detonation wave number, direction, frequency, and individual wave speeds throughout experimental RDE operational windows. To do so, the diagnostic integrates image classification by a convolutional neural network (CNN) and ionization current signal analysis. Wave mode identification through single-image CNN classification bypasses the need to evaluate sequential images and offers instantaneous identification of the wave mode present in the RDE annulus. Real-time processing speeds are achieved due to low data volumes required by the methodology, namely one short-exposure image and a short window of sensor data to generate each diagnostic output. The diagnostic acquires live data using a modified experimental setup alongside Pylon and PyDAQmx libraries within a PYTHON *data acquisition environment. Lab-deployed diagnostic results are presented across varying wave modes, operating conditions, and data quality, currently executed at 3–4 Hz with a variety of iteration speed optimization options to be considered as future work. These speeds exceed that of conventional techniques and offer a proven structure for real-time RDE monitoring. The demonstrated ability to analyze detonation wave presence and behavior during RDE operation will certainly play a vital role in the development of RDE active control, necessary for RDE technology maturation toward industrial integration.* [DOI: 10.1115/1.4062182]

Keywords: rotating detonation engine, machine learning, modal classification, high-speed imaging, neural network, combustion and reactive flows, experimental/measurement techniques

Introduction and Background

In recent years, the possibilities of higher thermodynamic efficiency and power output have led to increasing interest in the field of pressure gain combustion (PGC). Currently, a majority of PGC research is concerned with rotating detonation engines (RDEs), devices that theoretically achieve pressure gain through continuous detonation around an annulus, having lower entropy generation compared to Brayton cycle combustors. RDEs are being studied for future implementation in gas turbines, where they would offer efficiency gains in both propulsion and power generation turbines. Much diagnostic work has been done to investigate the detonative behaviors within RDEs, including point measurements, optical diagnostics, thrust stands, and other methods. As laboratory RDE operation becomes more reliable, run times increase in experimental settings, and industrial applications become more plausible, real-time monitoring of combustion behavior is a crucial step toward controlled RDE operation. This study aims to develop a real-time computer vision technique to monitor detonation wave behavior using an image classification convolutional neural network (CNN) coupled with high-speed measurement of flame ionization.

Annular RDEs rely on uninterrupted injection of fuel and oxidizer to maintain continuous detonation waves within a cylindrical annulus. A general characterization of this behavior, shown in Fig. 1, includes reactant (fuel and air) injection at the base, creating an unburned fill region which is consumed by the azimuthally rotating detonation front [1] with products flowing axially through the exhaust section. The graphic in Fig. 1 shows just a single detonation wave, however multiple co- and counter-rotating (CR) waves are possible. Both wide-field and narrow-field/point-source optical techniques attempt to capture this behavior through imaging along or perpendicular to the axial direction at the exhaust in Fig. 1, referred to as down-axis or transverse imaging, respectively.

[1]Corresponding author.

Manuscript received June 22, 2022; final manuscript received March 14, 2023; published online April 24, 2023. Assoc. Editor: Qiang Zhang.

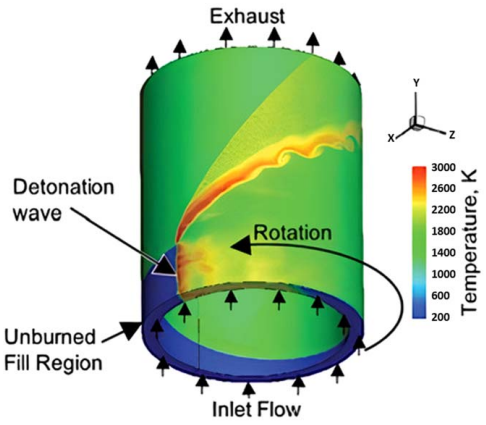

Fig. 1 General characteristics of RDE combustion [1]

Although many measurement techniques have been successfully implemented in experimental RDE facilities, the use of high-speed imaging boasts the unique benefit of high spatial resolution across the entire annulus.

Rotating Detonation Engine Data Analysis Methods. Within the RDE research community, techniques that analyze temporal (time series measurement including narrow-field/point-source optical), and wide-field optical data are utilized to classify and study the behavior of detonation waves within the RDE annulus. Time series data may include high-frequency data from pressure and heat flux sensors, ion probes, and other diagnostic sensors. Narrow-field or point-source optical diagnostics such as flame chemiluminescence by photomultiplier tube or spectrometer that integrates the signal across a sample region without providing spatial resolution are also considered time series data within the context of this study. Both optical and temporal data offer different benefits, complexities, and potential longevity to advance RDE TRL. Temporal data have been analyzed to determine wave modes and dynamics by way of fast Fourier transform (FFT), autocorrelation, cross-correlation, and other methods [2–7]. However, analysis of temporal data is often performed alongside, or verified by, optical techniques which offer the confidence of spatial resolution for determining wave number and direction (mode).

Down-axis high-speed images are commonly used to track detonation wave propagation through time. Data processing methods using pixel intensity offer information on the wave number, direction, and velocity. A series of down-axis images may be "unrolled" to create what are commonly referred to as *Detonation Surfaces* or *X-t* plots by concatenating polar pixel intensities which can be used to determine detonation wave speeds [2,8,9]. Example detonation surfaces for two counterclockwise (CCW) and three clockwise (CW) wave modes are shown in Fig. 2. Each of these techniques quantify detonation wave speeds and frequencies but require a series of 100 images or more and can only be performed in post-processing. Since the FFT limits the resolution to which the wave frequency can be estimated, the Hough transform (HT) was used to determine average wave property values. Hough transforms are commonly used in image processing to detect lines or edges within an image and have previously been used in similar RDE image processing efforts [2,4,9]. The Hough transform of the detonation wave matrix associates the trace of each wave with an identified line, which can be seen in Fig. 2. Wave direction on *Detonation Surfaces* is determined by the sign on the slope of the Hough transform lines, and the wave speed can be determined by the magnitude of the slope of the HT lines and spacing between lines provide an indication of the number of waves.

Other studies have utilized more optically accessible RDE designs to capture transverse images, or those perpendicular to the annulus axis. Transverse images have been used in conventionally cylindrical RDEs to characterize detonation structure axial and longitudinal variations [10]. Transverse imaging has also been used in "racetrack" RDEs, which has an annulus geometry that includes a straight section between two half-circles resembling a racetrack, to inspect non-ideal detonation behaviors including parasitic combustion, commensal combustion, shock structure, and other effects of vitiation [11,12]. Each of these optical studies are dependent on images captured with expensive high-speed camera systems capable of frame rates in excess of 50,000 fps, generating large volumes of data which must be post-processed. To analyze large data quantities more efficiently than current techniques, and possibly in real-time, machine learning techniques may be employed [13].

Classifying wave modes through down-axis image analysis has been the goal of multiple studies. However, recent methods developed by the current authors were the first to do so using CNNs, deep learning algorithms, applied to single images, reducing computational time significantly [13,14]. These developed CNNs can be executed to determine RDE wave modes through either classification of single images, or via object detection to track wave location within individual images. The first of these CNNs, used for image classification, is specifically used as a preliminary building block to the current method, which aims to create a real-time RDE diagnostic deployed in the lab environment. Neural networks may also be applied to RDE time series data such as pressure and ionization current (ion probe) data to determine active wave mode within the RDE. As time series point measurements are widely common in research and across many industries, extensive work has been completed to develop more efficient means of analysis using deep learning approaches. A recent study [15] detailed the training of a series of time series classification (TSC) deep neural networks (DNNs) which can classify the number and direction of waves within the RDE using univariate and multivariate pressure and ion probe datasets. The developed and trained DNNs were shown to have classification times that may also potentially be used for real-time wave mode characterization. Further details of analysis methods developed by the authors which employ neural networks for the analysis of experimental RDE data are presented in the following subsections.

Convolutional Neural Network Applications. The benefits of machine learning methods have been utilized in a variety of studies across the combustion community. As an early example, Santos-Victor et al. [16] demonstrated that flames within a glass furnace can be classified via computer vision to determine the number of active burners as well as the reactant flowrate. Grogan and Ihme [17] used machine learning to investigate the probability of predictive parameters for irregular combustion regimes and detonation sensitivity to heat release. Barway et al. [18] used artificial neural networks to develop a data-driven approach to combustion regime classification within the complex structure of detonation waves. Rezzag et al. [19] investigated instantaneous detonation wave speeds in post-processing using *k*-means clustering. As discussed earlier, the current authors have leveraged neural networks for RDE image classification [13], object (wave) detection [14], and time series classification [15] as efforts contributing to the development of a suite of viable RDE real-time diagnostic techniques, reviewed herein.

Image Classification Convolutional Neural Network. Since traditional feature extraction and image analyses are time consuming and computationally expensive processes, they are being widely replaced by various deep learning algorithms such as CNNs, which are well understood tools and often used for rapid feature extraction and image classification. CNNs perform feature extraction by using non-linear activation functions to filter features of an image or other data type, utilizing only relevant regions, as opposed to repeatedly processing the complete image. This enables a drastic reduction in

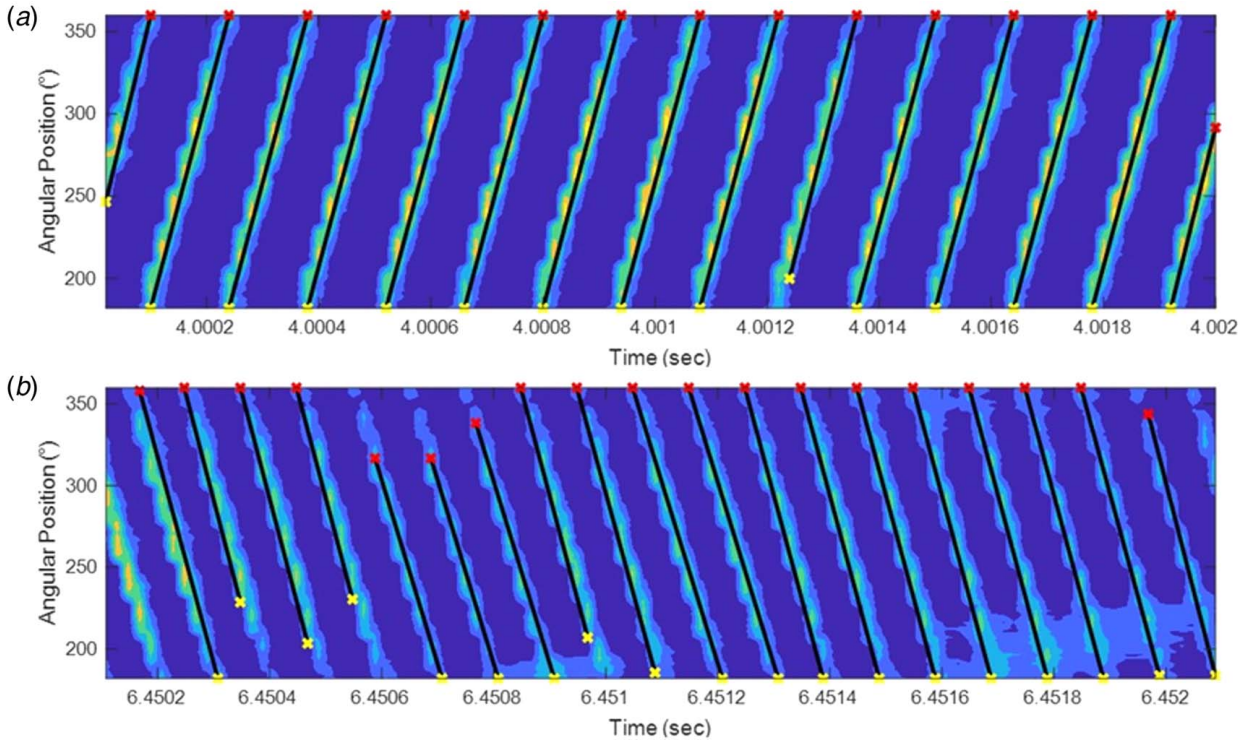

Fig. 2 Detonation surface with overlaid Hough transform lines used to identify (*a*) 2 CCW mode and (*b*) 3 CW mode [2].

memory requirements and computational times for analyzing a large number of images. CNNs excel at analyzing images for categorical classification. Analysis is accomplished by taking an input image and applying a set of trainable weights and biases to various aspects in the image, allowing the neural network to differentiate between the various features of an image.

In an effort to address the need for more high-speed diagnostics which can be operated in real-time, computer vision CNNs were applied by the current authors in past studies to down-axis RDE images for image classification and object detection. The first study surveyed five CNN architectures for image classification, and demonstrated that the number and direction of waves within an RDE annulus can be best classified by a SqueezeNet architecture [20] for a single image at accuracies exceeding 98% with a classification rate exceeding 33 fps (less than 30 ms per frame) [13]. The trained SqueezeNet network is used as a component of the proposed diagnostic throughout the current study and is trained to classify ten unique wave modes. Each wave mode, shown in Fig. 3, differs in number of detonation waves and rotational direction.

In Fig. 3, the label on each image refers to number of detonation waves, and whether the waves are rotating CW, CCW, or counter-rotating (CR). The last mode (Def) is a non-detonation mode representing deflagration. Although the number of waves present in each example is obvious to the human observer, the wave directions can

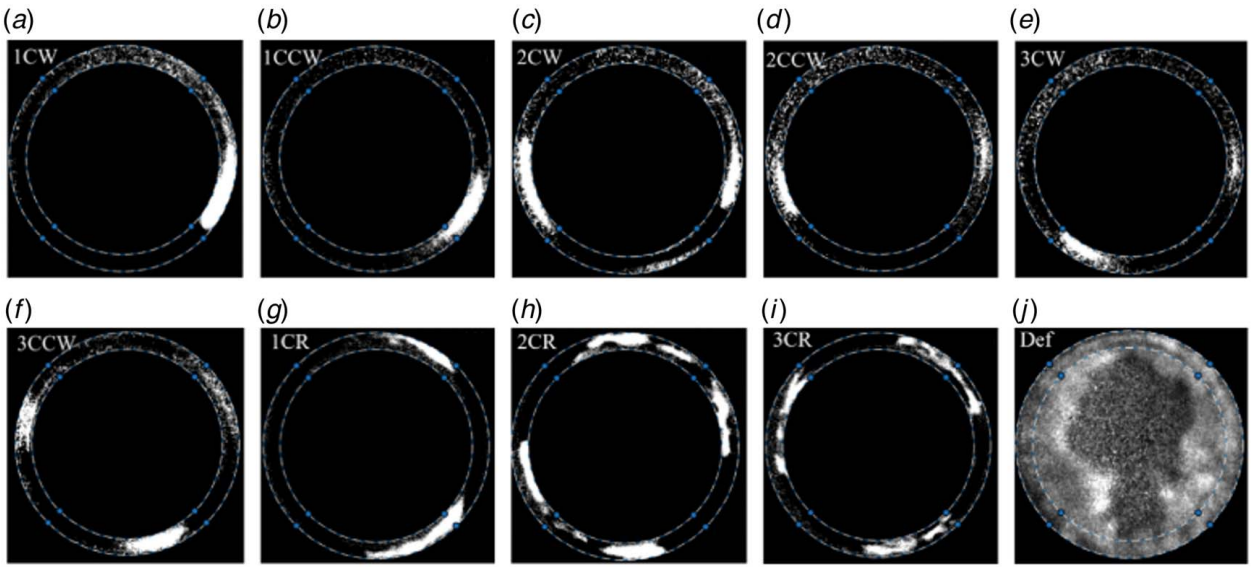

Fig. 3 Samples of successfully classified modes by CNN including: (*a*) 1 CW, (*b*) 1 CCW, (*c*) 2 CW, (*d*) 2 CCW, (*e*) 3 CW, (*f*) 3 CCW, (*g*) 1 CR, (*h*) 2 CR, and (*i*) 3 CR wave modes as well as (*j*) deflagration [13]

be inferred according to the wave profiles, which are utilized by the CNN feature extraction to properly classify wave modes.

To further acknowledge the intensity profile differences of each wave direction, Fig. 4 shows pixel intensities along the center radius of the annulus plotted against azimuthal location. Intensity profiles for each rotational direction are similar in structure, but profile characteristics occur in a reversed order along the azimuthal path, indicating opposite directions. In both instances, an abrupt spike in intensity caused by the blunt face of the detonation front is followed by a slow decay caused by the trailing profile. Although the general features are similar across waves, the appearance of waves throughout various operational periods will vary due to wave strength, chemiluminescent emission intensity, local equivalence ratio, and many other factors. Figure 4 shows two similar wave modes, but the CW wavefront is not as clearly defined as the CCW wavefront. The ability to discern these subtle differences across images by analyzing both low- and high-level features is the strength and goal of the applied neural network. Note that the intensity trends plotted in Fig. 4 are not an input for the CNN. Instead, the intensity plots are only meant to validate the existence of differing wave profile features utilized by the CNN.

Object Detection Method. Following the success of image classification CNN methods, the capabilities of computer vision applied to down-axis RDE images were extended to an object detection CNN architecture [14]. Detonation waves within a single RDE high-speed image were detected and annotated using the you only look once (YOLO) architecture [21]. Figure 5 illustrates an example of the object detection capabilities utilizing the YOLO architecture. The progression of annotation centroids was used to calculate wave velocity from frame to frame through a series of images to determine an average wave velocity. Using this method, the selection of annotation box sizes through manual annotation affects various performance metrics of the CNN. Specifically, larger bounding boxes are more effective for determining wave direction, while smaller bounding boxes were more accurate in calculating wave speed. While the locations of each wave may be tracked through time to determine frame-to-frame wave velocity, a capability not directly offered by image classification, it is done so at a slower classification speed than the SqueezeNet architecture.

Time Series Classification Method. Time series classification is a longstanding challenge in data mining, which aims to probabilistically determine the correct label of univariate or multivariate time series. Univariate datasets can be generalized as a collection of vectors containing data from a single sensor throughout time. Multivariate datasets are structured as matrices where in addition to the dimension of time, a second dimension is added for the inclusion of additional sensors. This data structure is illustrated in Fig. 6 [22]. As the number of sensors increases, so does the size of the multivariate set by stacking traces recorded simultaneously along the time axis. Applied to RDE time series data, the benefit of multivariate datasets is a result of added spatial resolution as well as varying sensor types. A number of methods to solve time series classification have been developed and considered. Some examples of popular and traditional solutions included nearest neighbor classifiers joined with a distance function, decision tree, support vector machines, HIVE-COTE [23], and many others [22].

Increased accuracy of these methods results in increased processing time, often to the point of impracticality. An alternative to

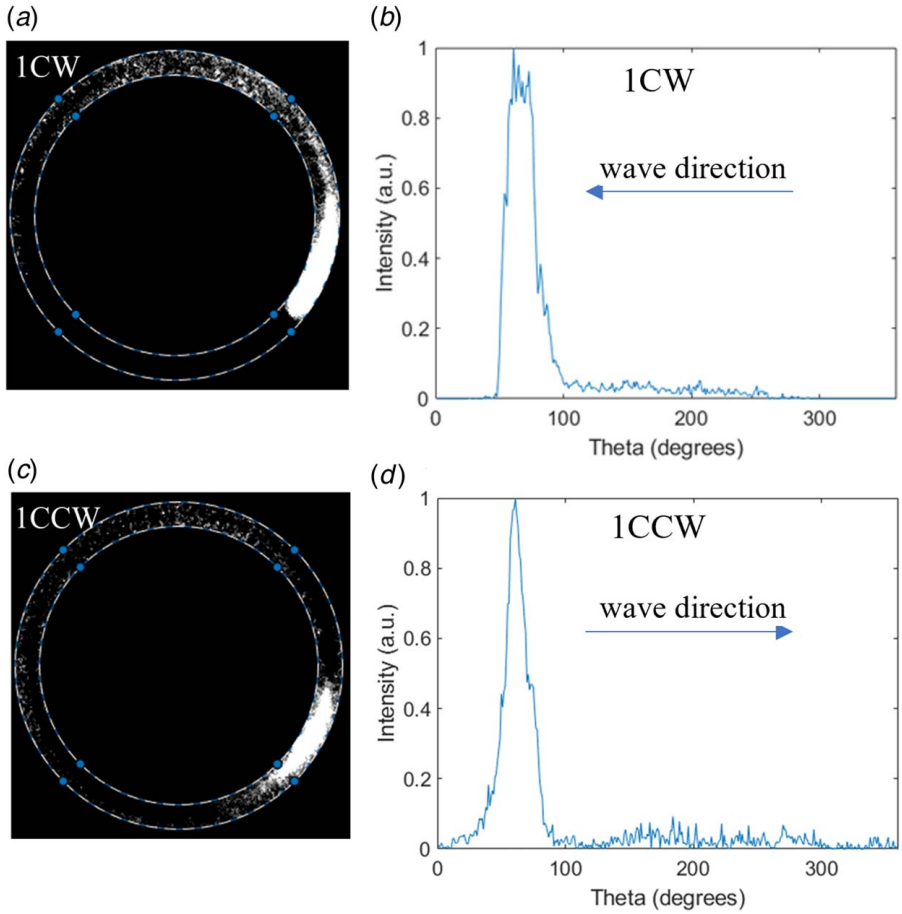

Fig. 4 Downstream images of modes (*a*) 1 CW and (*c*) 1 CCW, paired with pixel intensity along center radius of annulus plotted against theta for (*b*) 1 CW and (*d*) 1 CCW [13]

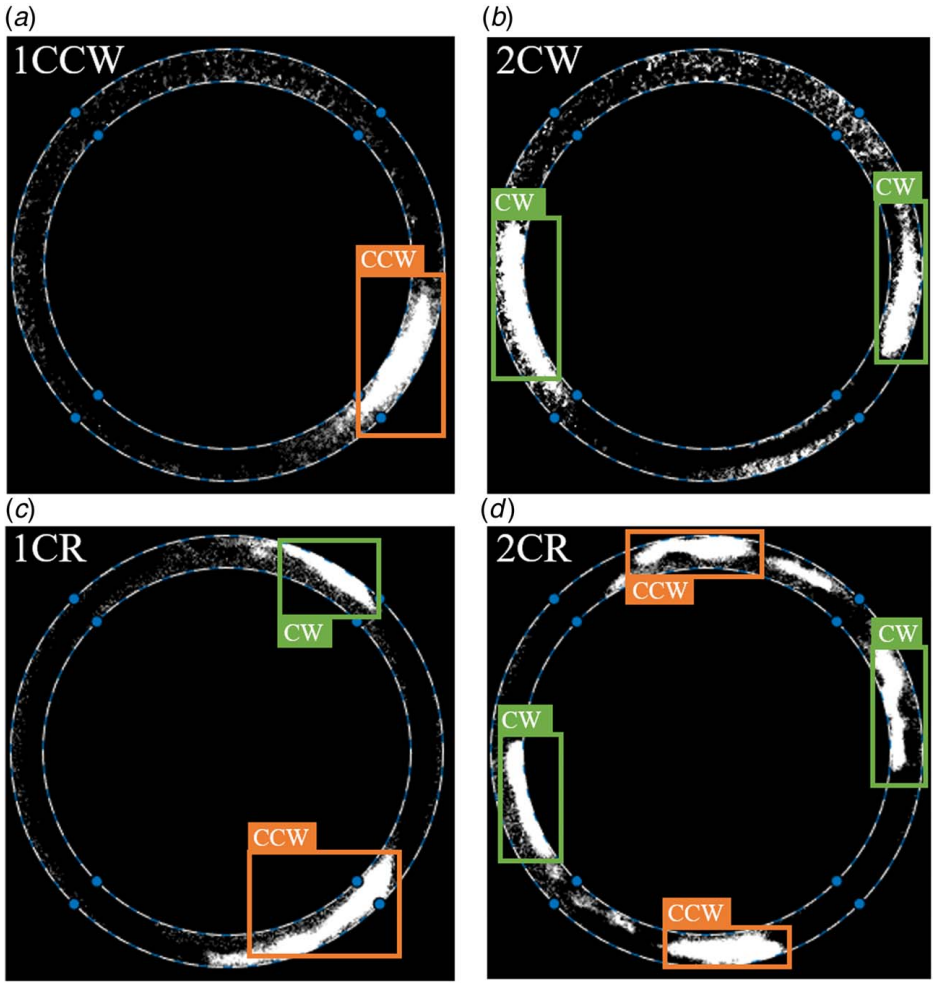

Fig. 5 Annotation of RDE down-axis images of (*a*) 1 CCW, (*b*) 2 CW, (*c*) 1 CR, and (*d*) 2 CR modes [14]

traditional TSC, DNNs were applied to perform TSC on experimental RDE pressure and ion probe data recorded at 250 kHz [15]. Data labels indicating wave number and directionality for each sample window were generated through analysis of simultaneously captured down-axis images, offering spatial certainty typically absent in time series analyses. The targeted output of modal classification mirrors the current effort, with a potential benefit of reduced data dimensionality and hardware requirements by developing a diagnostic which can operate independent of down-axis imaging. Similar to the current study, the deployment of the TSC network in the laboratory environment will be performed as a future work and compared to the results presented here as competing means of achieving intelligent control of fuel schedules. Multiple datasets were created to study the advantages of univariate and multivariate time series and were each used to train three unique architectures to determine the optimal network arrangement. The DNN architecture developed follows the TSC framework, as shown in Fig. 6. The time series, either univariate or multivariate, is fed to the DNN which performs non-linear transformations according to the prescribed architecture resulting in a probability distribution over the classes present in the dataset. Example data used in the study, including high-frequency ion probe data from operational windows consisting of two and three waves, is shown in Fig. 7.

After surveying 24 dataset-network combinations, a five-layer fully convolutional network [24] trained on multivariate dataset with data lengths of 200 samples was chosen as the preferred network. The final network was reported with training accuracy, validation accuracy, and classification time of 100%, 91.36%, and

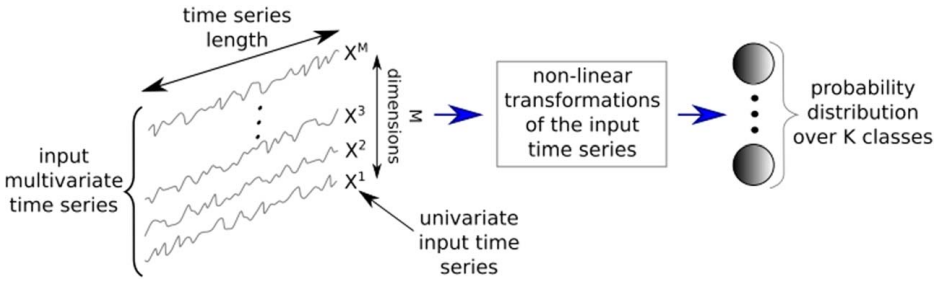

Fig. 6 Generic DNN TSC framework for multivariate time series [22]

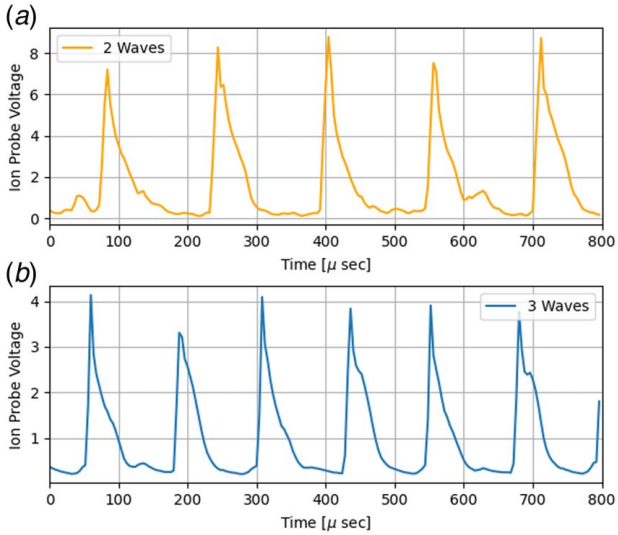

Fig. 7 Example ion probe voltage readings for (*a*) two and (*b*) three wave modes throughout 200-sample windows

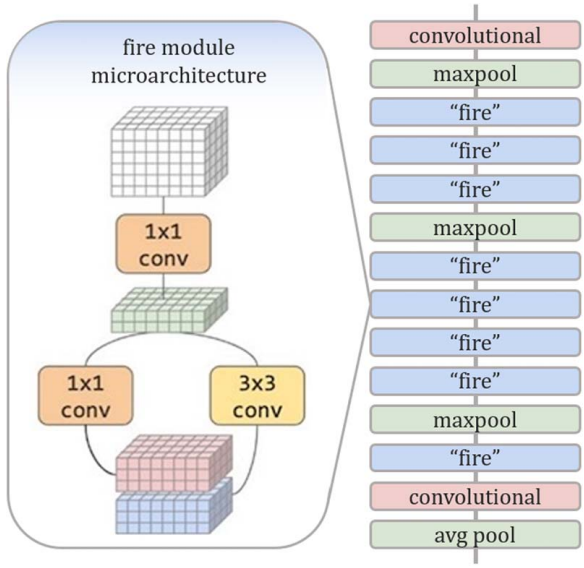

Fig. 8 SqueezeNet fire module (left) expanded from SqueezeNet architecture visualization (right) [20,25]

28.76 ms, respectively [15]. Within the study, which aimed to develop a TSC network as a component of an RDE real-time diagnostic, classification time was of highest importance when comparing networks. While this TSC network boasts more efficient classification times than the SqueezeNet image classification network due to reduced data dimensionality, accuracies on test data show lower precision. The chosen network will be employed as a component of a real-time RDE diagnostic in a manner similar to the current study in a future work.

SqueezeNet Architecture. Of the three methods developed for real-time diagnostics discussed above, each offers various advantages which should be studied and compared in the lab environment. The current work aims to do so for the image classification SqueezeNet architecture. Details of the architecture, and CNNs in general, are briefly detailed in this section. CNN designs are inspired by the connectivity patterns of neurons in the human brain as the architectures attempt to simulate human visual cortices. Images or time series data are broken down into discrete areas known as receptive fields in which neurons respond to stimuli only in that field. These fields are overlapped together to cover the entire data field, and by breaking down the data into these fields it is possible to draw out the spatial and temporal dependencies by applying relevant filters.

The strength of CNNs over traditional neural networks is the application of convolutional layers which work by sliding a filter over a finite pixel or sample region and taking the dot product between filters to produce an activation map. As the CNN becomes deeper with multiple convolutional layers, the dot product of the deeper layers inherits dot products of the previous convolutional layers allowing low-level features to be built into high-level features. The ability of these networks to perform parameter sharing while having local connectivity reduces the number of trainable parameters in the system, i.e., neuron weights, leading to a more computationally efficient system [13].

Another important aspect of CNNs is the use of max pooling layers that reduce the spatial dimensionality of an input image. Pooling layers play a key role in the computational efficiency of CNNs by reducing the dimensionality of the input data resulting in fewer parameters and thereby lesser computational expense. These max pooling layers operate as independent layers from the convolutional layers. Max pooling layers achieve dimensionality reduction by applying a filter of a specified size to an input image and taking the max pixel value within the filter location. The filter is then moved by a pixel distance, defined as a stride length, where the filter is again applied. The process is repeated until the entire image has been filtered and reduced.

The arrangement and specification of convolutional, max pooling, and other layers are referred to as the CNNs architecture. There are a multitude of unique architectures that exist in the literature consisting of various combinations of filters, layers, neurons, and other trainable parameters, termed hyperparameters, that all attempt to achieve the same goals as quickly and efficiently as possible. Hyperparameters are tunable parameters that can significantly affect the performance of a CNN. Typical hyperparameters are learning rate, activation function, kernel initializers, stride length, kernel size, and pooling size. The network employed throughout the current study, SqueezeNet, is illustrated with an expanded view of the namesake fire module in Fig. 8.[2] SqueezeNet is a unique architecture in the CNN design space, as it was developed to achieve the same accuracy as other popular architectures, but with fewer parameters and a smaller model size by incorporating a building block referred to as a fire module. The architecture is comprised of a single convolutional input layer followed by eight fire modules and ending with another single convolution layer. The fire module, whose microarchitectural view is expanded in Fig. 8, utilizes *squeeze layers* of 1×1 convolutional filters to reduce parameter volume as well as to decrease the number of input channels to the downstream *expand layers* of 3×3 convolutional filters. Max pooling is performed after the first, fourth, and eighth layers, and a global average pooling after the final convolutional layer, each at a stride of two pixels. The output is fed to a softmax function, typical for classification problems. Further information detailing the SqueezeNet architecture can be found in the original literature [20], or in the previous work of the current authors [13].

The work documented within this paper aims to deploy a CNN, trained within the National Energy Technology Laboratory (NETL) RDE research effort, as a real-time diagnostic component in the laboratory environment. The CNN utilized is trained with over 100,000 images to classify wave number and direction in images at accuracies exceeding 98% [13]. Within the lab, the diagnostic utilizes

[2]Portions of this page are modifications based on work created and shared by Google and used according to terms described in the Creative Commons 4.0 Attribution License. https://codelabs.developers.google.com/codelabs/keras-flowers-squeezenet#6

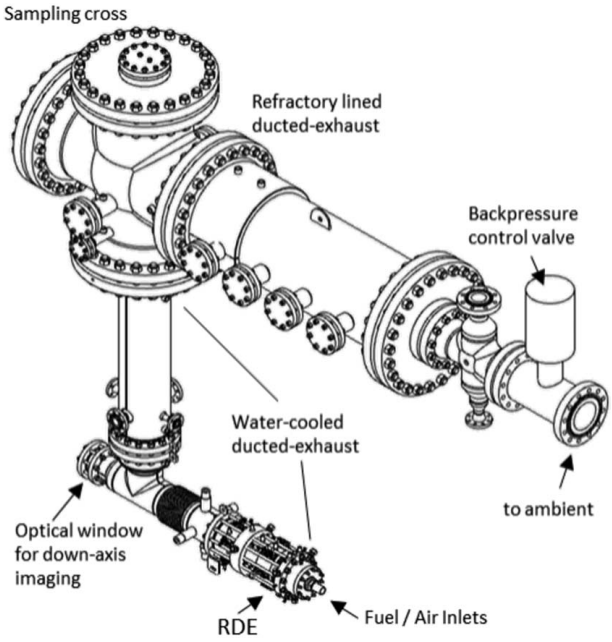

Fig. 9 Water-cooled RDE with ducted exhaust at NETL

CNN output wave classifications alongside analysis of ion probe data to more quickly and accurately determine wave speed and frequency. As a principal component of the diagnostic, the SqueezeNet model is loaded within the experimental data acquisition system in an effort to achieve real-time RDE wave mode characterization during experimental testing. Diagnostic results presented represent data output during RDE operational windows without post-processing, offering a potential means of intelligent fuel control in future studies. The ability to extract information regarding detonation wave number and frequency during RDE operation using CNNs at high accuracies and classification speeds will serve as a benchmark for RDE diagnostics and machine learning applied to pressure gain technology.

Experimental Setup

Tests performed in this study were conducted in a water-cooled, ducted-exhaust annular RDE, which is installed in the High-Pressure Combustion Research Laboratory at the US Department of Energy, NETL. A graphical representation of the experimental setup showing the cooled RDE along with the exhaust duct and backpressure control valve is shown in Fig. 9. The combination of ducted exhaust and backpressure control valve allows the pre-combustion pressure to be regulated in the exhaust at pressures ranging from ambient to 20 bar. Water-cooling of the RDE and exhaust permits individual run times of 20 s. This is sufficient to bring the combustor to a thermally stable state, although material temperatures of the exhaust downstream of the RDE continue to rise throughout the test, causing a continued increase in exhaust pressure above the combined pre-combustion setpoint and pressure as a result of sustained detonation.

A cross-sectional view of the RDE and profile view of axial air injection, combustion channel, and exit nozzle are shown in Figs. 10 and 11. The 119.5 mm long RDE utilizes an axial air injection configuration with an injection area, $A_{3.1}$, of 16.23 cm^2, an outer diameter of 149 mm, and a combustion channel width of 10 mm, resulting in a ratio of channel area to injector area ($A_{3.2}/A_{3.1}$) of 2.7. At the end of the combustor is an exit nozzle, choking the flow by applying additional pressure in the combustion channel independent of the backpressure control valve. The exit nozzle has a minimum area of 33.8 cm^2, creating an exit area to channel area ratio ($A_8/A_{3.2}$) of 0.76. Immediately downstream of the exit nozzle is an exhaust diffuser whose purpose is to slow the flow from the RDE to a hypothetical turbine inlet. Additional details on the diffuser are not provided as its influence is not significant to this study, although it was installed while testing. After the diffuser, the exhaust duct opens to a diameter of 154 mm. Hydrogen fuel is injected through 120 evenly spaced jets on both sides of the air inlet, totaling 240 jets, located just downstream of the air inlet throat where the cross-sectional area is minimal. Each jet has a diameter of 0.75 mm offering a total fuel injection area of 1.06 cm^2.

The experimental configuration of the RDE permits the installation of a variety of transducers with data sampling rates of 1.25 Hz (very slow-speed), 5 kHz (slow-speed), 250 kHz (mid-speed), and 1 MHz (high-speed). Relevant to this study is the use of an ion probe to measure ionization current, sampled at 250 kHz, centered approximately 4 mm downstream of the tip of the axial air injector, permitting sampling within the detonation wave. Output from the ion probe, measuring chemi-ionization from the detonation wave, is acquired using a National Instruments cDAQ-9188 chassis and NI 9223 module which is independent of the primary data acquisition performed with a NI PXIe-1082DC chassis and NI PXIe-8880 controller along with a series of NI analog input modules.

A 90 mm diameter fused quartz window is located approximately 1 m downstream of the RDE exit just past a 90 deg elbow in the main exhaust duct. The window typically provides access for capturing high-speed video at 60k fps using a Photron FASTCAM

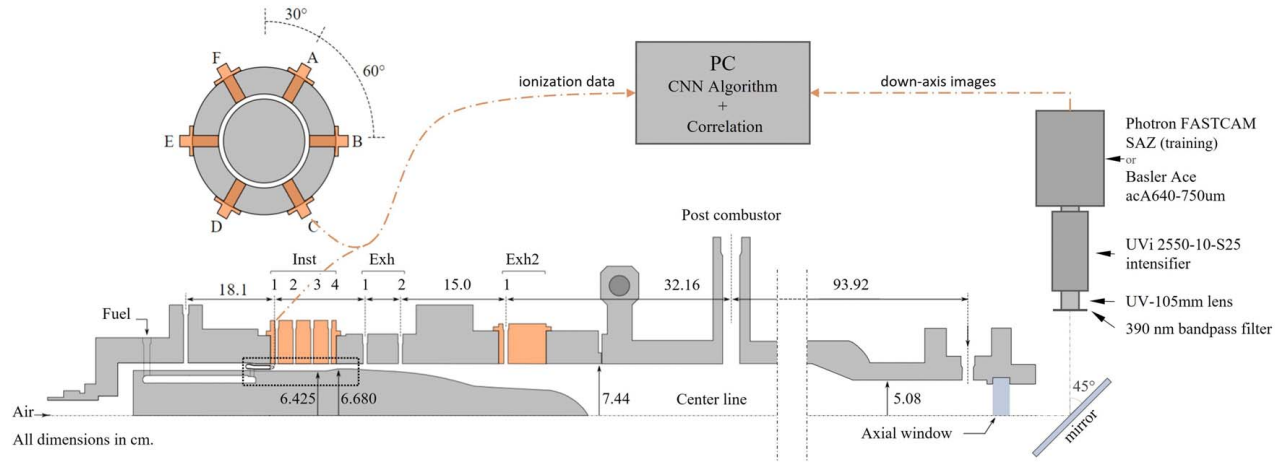

Fig. 10 Cross section water-cooled RDE showing axial injection, sampling port nomenclature, exit nozzle, downstream diffuser, camera alignment, and data acquisition setup. Box indicates boundary for Fig. 11.

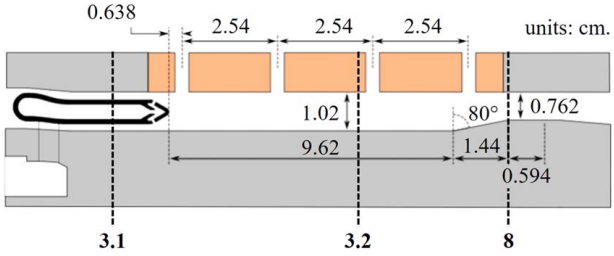

Fig. 11 Profile view of axial air injection, combustion channel, and exit nozzle with station designations at the air injector throat (3.1), combustion channel gap (3.2), and exit nozzle throat (8) [26]

SAZ. The Photron camera is utilized to capture down-axis images of the detonation wave required to train the CNN. For this test series, the Photron camera is replaced with a 10-bit Basler Ace acA640-750um area-scan camera with a maximum resolution of 640 × 480 pixels. The camera is connected to an Invisible Vision UVi 2550-10-S25 intensifier, a Nikkor UV-105 mm lens, and a 390 nm bandpass filter with a full width-half maximum of 125 nm to primarily limit observation to OH* chemiluminescence that dominates the combustion wave, depicted in Fig. 10. Although the camera has a maximum frame rate of 751 fps, the camera is triggered at each diagnostic iteration. In order to prevent smearing of the detonation wave, the intensifier gate width is limited to 12 μs.

Image and ion data collection are triggered and performed using the Basler Pylon [27] and PyDAQmx [28] libraries, respectively, within a PYTHON environment throughout RDE operational windows. The current study relies on the partially modified experimental setup but intends to develop a monitoring technique feasible for ongoing studies and future adaptations for active control using instrumentation widely available within existing experimental RDE facilities. While instrumentation schemes of productions engines remain unclear, the current structure of high-speed data fed to machine learning algorithms is expected to remain applicable throughout the industrial integration of RDE technology.

Methodology

The methodology necessary to achieve real-time diagnostics consists of three distinct portions: training of a CNN for image classification, integration of ion probe data, and advancement of data acquisition and processing techniques for real-time data processing and reporting. Of these three, the final effort of advancement toward real-time monitoring and classification of RDE modal behavior in the laboratory environment is the primary thrust of the current study. The novelty of the current work lies in the method of experimental setup adaptation, and integration of various data analytics to provide real-time monitoring of RDE behavior, an ability not obtainable via other methods to date. The first portion of the overall methodology is substituted by a previously developed CNN, which was trained to classify the number and direction of counter- and co-rotational detonation waves in individual images of an uncooled RDE [13]. The preferred network developed in that preliminary study uses an architecture named SqueezeNet, which was trained to classify ten RDE wave modes from down-axis images. The finalized architecture and weights are used in the CNN inference mode throughout the current study. A brief functional overview of the steps taken to generate the utilized CNN is presented here, while a more in-depth discussion of the theory, dataset generation, training method, and architecture selection recommendations can be found within the previous work.

To elaborate, the previous work provided a CNN, which was trained and validated using a set of manually classified images. In that work, the performance of the network, being image classification only, was documented for training and validation images. This included accuracy and speed of image classification alone. Within that work, no efforts to obtain wave velocity measurements, or any other real-time results were performed. That same CNN now serves as a single component of the current method. In other words, the method outlined in this section includes subsections CNN Image Classification, which is adopted from the previous work, while subsections Time Series Data Integration and Real-Time Processing and Lab Integration are entirely unique, and are the thrust of the study. Execution of this new methodology leads to real-time results, which have never before been attainable, and are thought to be a required achievement to develop an active control framework.

Convolutional Neural Network Image Classification. Among machine learning methods, a major distinction is made between supervised and unsupervised learning. Unsupervised learning requires input data with no associated output or labeling, and aims to discover underlying data patterns and groupings. Supervised learning relies on labeled input-output data that is associated with a known output or classification to train the network. The creation of the CNN for the present work relies on a supervised learning process involving four major phases: imaging, CNN training, CNN validation, and CNN end usage. The order of each phase and notable substeps are visualized in Fig. 12. The CNN itself is an arrangement of max pooling, convolution and fire layers, referred to as the architecture. While many unique architectures could perform the task at hand, selection of the SqueezeNet architecture [20] is based on classification speeds which far exceed that of other networks trained on the same image set [13].

To begin the imaging phase, a set of down-axis high-speed images must be manually labeled, or classified, according to their wave number and direction. The classified images are then partitioned into two subsets, the training image set and the validation image set, which contain 70% and 30% of the classified images, respectively. The next phase, CNN training, begins by shuffling the training images. This process is imperative as it is dual purposed: ensuring the model is incrementally analyzing images across the classification range, which limits possible bias toward individual classifications; and creates a nonsequential dataset, eliminating time dependencies from image to image. Shuffled images

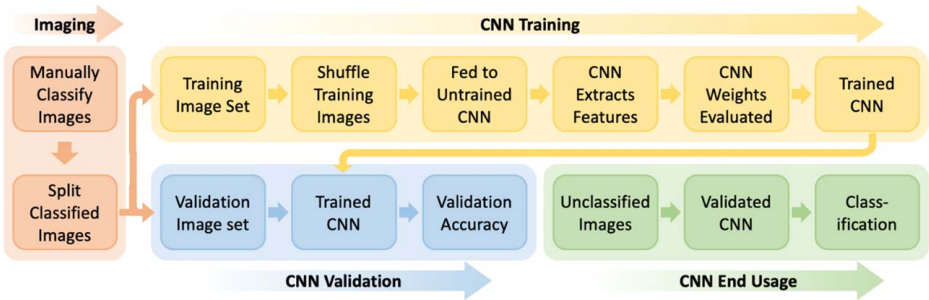

Fig. 12 CNN development methodology [8]

and their labels are then fed to the untrained CNN which executes feature extraction and updates its trainable weights. After every epoch, which is one complete evaluation of the entire set of training images by the CNN, the subsequent training accuracies are evaluated.

Simultaneously, the CNN validation phase works to evaluate the incrementally trained CNN by attempting classification of the validation image set without labels. The incrementally trained CNN predicts labels for each of the images, which are then compared to the known label to determine validation accuracy. Once the training and validation accuracies are found to be acceptable, the CNN is considered trained and validated, and can then be used indefinitely to evaluate unclassified images. It is important to emphasize that the first three phases indicated in Fig. 12 must only be performed once to develop a production CNN which can be used indefinitely as a tool to classify new, unlabeled relevant images. When dealing with CNNs in practice, there are three accuracy metrics: training, validation, and testing accuracy. Training and validation accuracies of the CNN, being 99.6% and 98.5%, respectively, are determined during the training regimen executed in the previous work [13]. Only testing accuracy may vary after CNN training and validation are finalized. The current work resides in the inference stage of CNN use, denoted CNN end usage in Fig. 12, where testing accuracy may with varying image similarity. Testing accuracy is expected to be less than training and validation, especially for images captured in a different manner than those in the training image set but should be sufficient for diagnostic purposes.

While development of an image classification CNN is pertinent to the establishment of the current methodology, its usage in isolation is limited to a sophisticated post-processing technique. The significance of the current work is rooted in time series data integration and real-time processing of live data via an altered experimental setup, which are outlined in the following subsections.

Time Series Data Integration. Analysis of high-speed time series data, such as pressure or ion probe, is commonly used to determine detonation wave behavior [7,29,30]. This process typically relies on cross-correlation or power spectral density analyses, which are then related to an estimated ideal velocity via Chapman–Jouguet (CJ) theory, a classical theory describing a thin detonation wave with infinite chemical reaction rate, to determine wave number and frequency [31]. As mentioned in the previous section, point measurements lack complete spatial resolution and may therefore confuse more complex modes or secondary behaviors. Additionally, those methods which rely only on time series traces may require large sampling sizes and will therefore be unlikely to reach real-time feedback capabilities.

However, with wave number and direction supplied by the image classification CNN, time series data may be quickly and certainly analyzed to determine wave frequency. To accomplish this, CNN image classification and time series data evaluation techniques can be integrated. First, using auto-correlation for a 200 sample-length window of ion probe data collected at a sampling rate (SR), of 250 kHz, the sample lag, τ, can be found. Using Eq. (1), the frequency of the ion probe signal, f_{ion}, can be found. While the frequency of RDE time series data is commonly found using an FFT, the resolution of an FFT is drastically reduced by shortened sample lengths. Auto-correlation resolution is proportional only to the sampling rate and is therefore more well suited for analysis of brief data windows, which are of interest due to the pursuit of a real-time diagnostic. Using Eq. (2), the wave number output from the CNN, m_{CNN}, is used alongside ion probe frequency and the nominal RDE annulus diameter, d_{nom}, to determine individual wave speed, U_w.

To visualize the proposed diagnostic data flow, a diagram is shown in Fig. 13, whereupon determining detonation wave number and rotation type from an individual image, a very short sampling of ion probe data is needed to find the wave velocity and frequency. Inevitably, the CNN will produce sporadic misclassifications. To address this issue, either a rolling or sliding window median of wave number can be used in place of m_{CNN} within Eq. (2). The results presented in the next section plot both median types and utilize a sliding window median with a width of seven iterations to calculate individual wave speed.

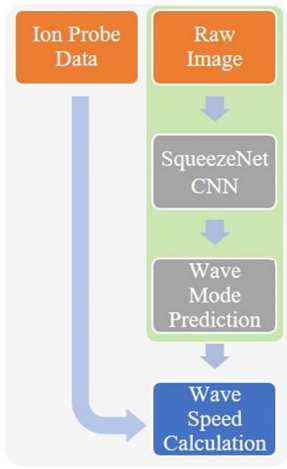

Fig. 13 Diagnostic data flow diagram

$$f_{ion} = \mathrm{SR}/\tau \tag{1}$$

$$U_w = \pi\, d_{nom} f_{ion}/m_{\mathrm{CNN}} \tag{2}$$

Real-Time Processing and Lab Integration. The data flow process illustrated in Fig. 13 is simple in nature once a CNN is trained for the specified outputs and can be used as a post-processing technique to evaluate the RDE detonation wave behaviors within operational windows much shorter than other techniques. However, the objective of the current study is to develop a real-time RDE diagnostic. Therefore, the ability to collect data and execute the process in Fig. 13 while the RDE is running is imperative. It is important to note that this technique does not aim to analyze every image or every time series reading. Instead, for each iteration i, a single image is captured by the Basler camera at t_i and ion probe data acquired within a sample window of length ΔT_{Si}. The sample window length, ΔT_S, is equal to 200 samples at 250 kHz, or 0.8 ms. The time needed to acquire the data from the camera and sensor, image classification, and calculations will be performed, taking the time indicated as Δt_{Ci} in Fig. 14.

Using the single image and the short window of time series data, the diagnostic will output wave number, direction, frequency, and individual wave speed at each iteration. The next iteration will acquire the most recent data for the next loop, beginning at t_{i+1}. In general, this means that only one image at the beginning of each loop will be considered, and the ion probe data in the highlighted section are not considered. The summation of sample window length and calculation time, $(\Delta T_S + \Delta t_C)$, is the period at which the diagnostic output is reported. Therefore, the feedback frequency is equal to $1/(\Delta T_S + \Delta t_C)$. Reducing either time parameter directly improves feedback frequency with unique challenges and drawbacks. Decreasing sample window length, ΔT_S, is the simpler alteration, but reduces accuracy of the time series correlation.

In an effort to optimize both operations for accuracy as well as processing speeds, data treatment is kept to a minimum. Images fed to the CNN are adjusted using only a median blur digital filter. Prior to auto-correlation, ion probe data windows are filtered using a Butterworth digital filter with a filter order of five and a critical frequency of 6000 Hz normalized by the Nyquist frequency, being 125 kHz or half of the sampling rate. The critical frequency is the frequency at which the response of the filter is equal to the square root of 0.5. The filter gain response is plotted in Fig. 15.

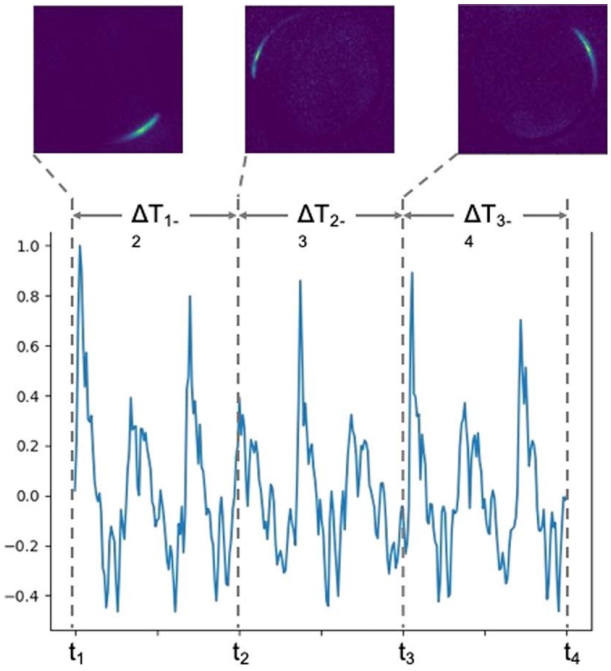

Fig. 14 Image and time series data sampling and integration

Finally, this technique is adapted to be executable within a PYTHON environment during RDE operation. The hardware used to acquire live data is detailed in the earlier Experimental Setup section. Prior to each diagnostic run, the environment session is established and prepared with all operations that precede diagnostic execution. Connections to the Basler camera, via the USB 3.0 connection, as well as the NI cDAQ chassis, via ethernet connection, are established and configured using Pylon and PyDAQmx libraries, respectively. Empty variables are created to store incremental diagnostic outputs and performance metrics, and the CNN model and weights are loaded into the environment. The completed CNN is small in memory space and can be uploaded and utilized with only a few lines of code. After initialization measures are complete, the environment session is prepared to perform the diagnostic during RDE operation. Throughout operation, all raw data as well as calculated values and timing metrics are recorded. Recorded data are saved after each run, and the environment session is reinitialized. Intuitively, these efforts will target the minimization of the shaded areas, or Δt_{Ci}, in Fig. 14 for higher feedback frequencies which is a crucial step in optimizing the system with the goal of achieving real-time monitoring within the RDE flow field.

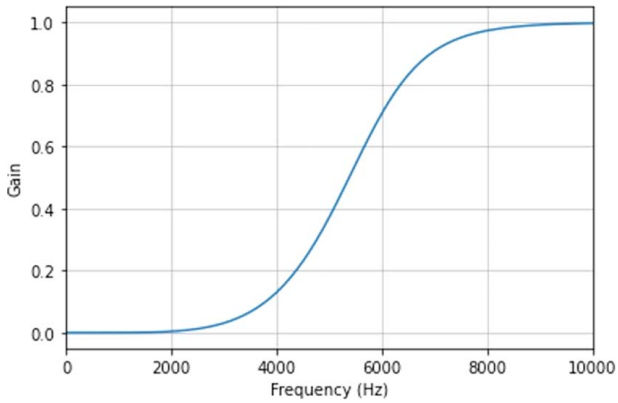

Fig. 15 Frequency response of digital Butterworth filter

Speed and accuracy of the method are vital to the overall thrust of the work: to monitor RDE waves during extended operational windows. Speed and accuracy are required, and offered in part by the CNN developed in the previous work [13]. The proposed framework, in which the CNN is a principal component, is novel to record image and ion data simultaneously while processing that data at timescales much smaller than the run time, and comparable to the control capabilities of the facility.

Results

A real-time RDE diagnostic technique is developed using an image classification CNN and correlation of high-speed ion probe data and is deployed in the laboratory environment. Advancement of RDE modal analysis beyond conventional post-processing speeds achieving live data output capabilities during operational windows of an experimental RDE is targeted as a critical step in technology maturation. The diagnostic requires short-gate, 10 μs, intensified down-axis images and short windows of ion probe data. By executing the method described in the previous section, each iteration provides wave number, wave direction (not plotted), iteration time, wave frequency, and individual wave velocity. Each of these values are recorded over individual RDE runs and plotted alongside example images and ion probe data in the figures to follow. It is important to note, that because this study is concerned with the performance of a real-time diagnostic, no post-processing or digital filtering has been performed to the presented results. All classifications and calculations plotted below represent the output of the diagnostic during live RDE operation. In each subplot, overall medians are plotted as solid lines, and the sliding window median of wave number is plotted as a dashed line. The sliding window median is used to relate ion probe frequency, calculated through auto-correlation, to the individual wave velocity using Eq. (2). A single image and ion probe window are recorded for each iteration. However, a subsampling of four images and one ion probe window is plotted in each diagnostic example.

Figure 16 shows a diagnostic output for a quasi-steady two-wave run whose operating conditions are an air temperature, T_{air}, of 320 °F, equivalence ratio, Φ, of 0.75, and initial backpressure, P_{back}, of 0 psig. Images in Fig. 16 on the upper right show a clear 2 CW wave mode, with an addition point of pixel intensity associated with a thermocouple. Images are 640 × 480 pixels with pixel depth of 10 bits. The utilized image classification CNN was trained on images from a Photron FASTCAM SAZ with a cropped size of 301 × 301 pixels. Therefore, images captured by the Basler camera are cropped to square proportions centered about the RDE annulus and resized to match the size and format of the desired CNN input.

The classification of wave number experiences occasional misclassifications of one wave, often when the pixel intensity and apparent size of the second wave are significantly less than the first. Even in instances of misclassification, the sliding window median (dashed line) reflects the true mode present with only a few points of error across a 17 s sampling (60 iterations).

Ion probe signals exposed to less extreme operating conditions and more stable wave modes display clean, well-defined peaks (lower right). This type of ion trace results in stable frequency outputs across the entire run, like what is shown in Fig. 16. The sliding window median is used to relate the frequency values, to individual wave speeds, averaging 6492 Hz and 1623 m/s respectively, and plotted in the bottom-middle portion of Fig. 16. The iteration time across this run averaged around 0.28 s, or 3.57 Hz, which is slightly higher than experienced across runs presented in Figs. 17–19.

The diagnostic has been evaluated over more than 100 runs. Figures 16–21 serve as a sampling of diagnostic outputs with the purpose of displaying the diagnostic performance across varying operating conditions, measurement quality, and wave modes. Figure 17 mirrors the format of Fig. 16, displaying the diagnostic

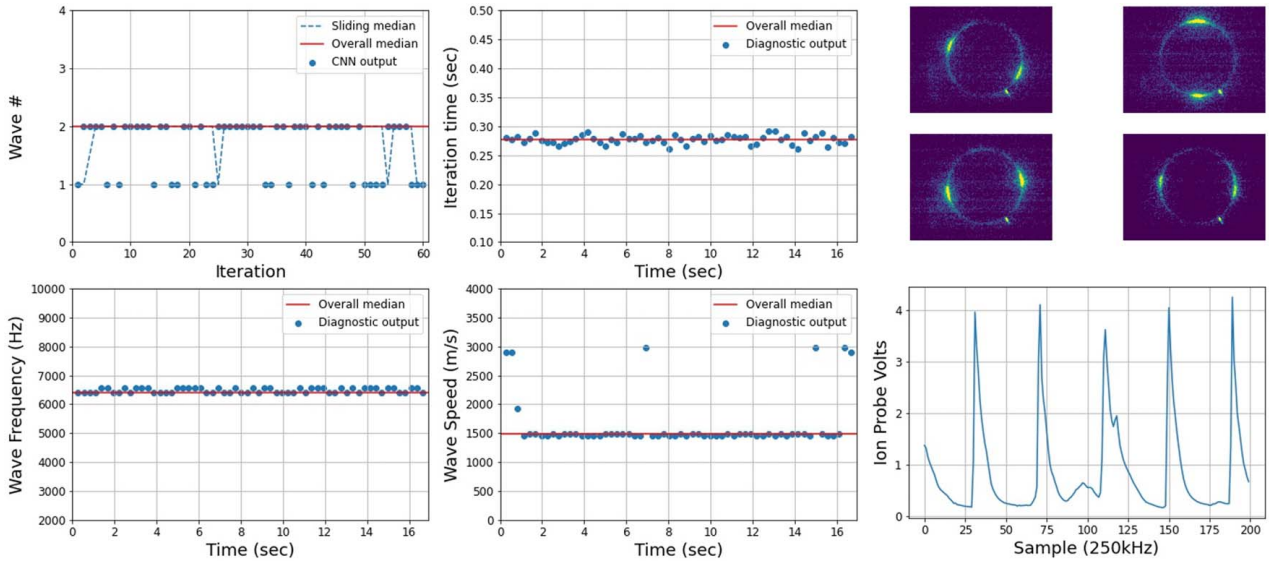

Fig. 16 Diagnostic output monitoring 2 CW steady waves with operating conditions: $T_{air} = 320$ F, $\Phi = 0.75$, $P_{back} = 0$ psig

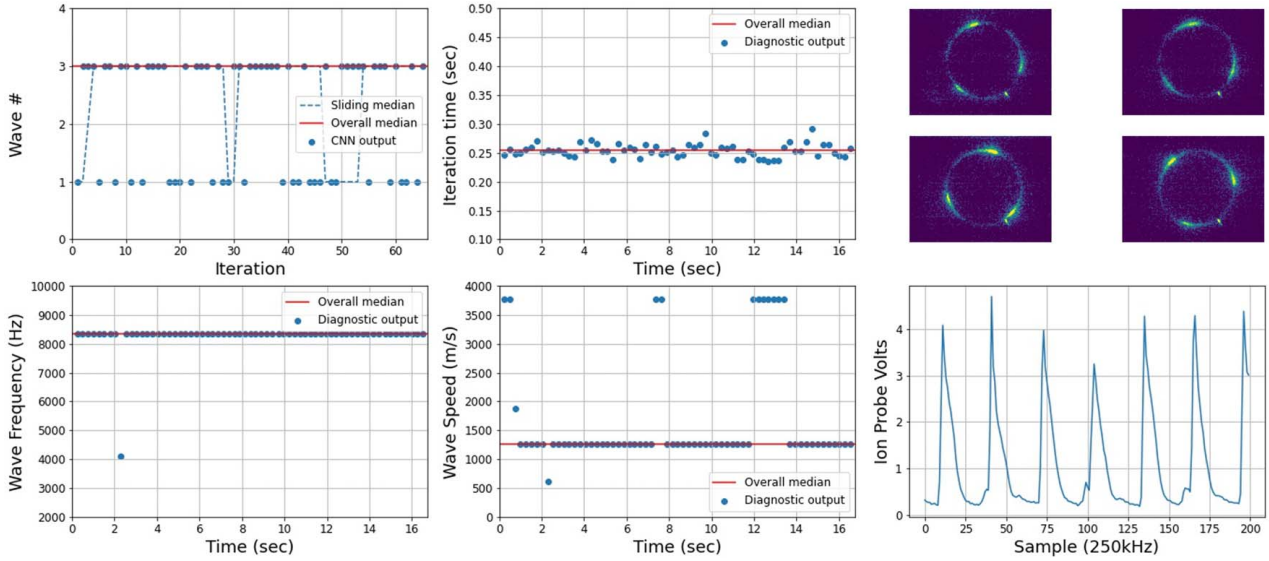

Fig. 17 Diagnostic output monitoring 3 CW steady waves with operating conditions: $T_{air} = 400$ °F, $\Phi = 0.75$, $P_{back} = 0$ psig

output across a steady three-wave operational window with conditions $T_{air} = 400$ °F, $\Phi = 0.75$, and $P_{back} = 0$ psig. Again, the images show a fairly clear wave mode, which is classified by the CNN with a fair degree of accuracy. In most cases of error, the sliding window median corrects the wave count. Misclassification of higher wave counts is expected as pixel intensity decreases with a decreasing wave strength given a constant gain setting on the intensifier. Autocorrelation of the ion signal results in a very steady wave frequency of 8333 Hz and resultant wave speed of 1257 m/s. Iteration times averaging 0.25 s led to a diagnostic feedback rate of 4 Hz.

Results presented have shown the performance across extended run times allowed by the water-cooled rig. Although the feedback rate could be improved, it still offers valuable information across shorter runs. Diagnostic outputs across a 5 s run with two waves present throughout are shown in Fig. 18. Operating conditions are $T_{air} = 320$ °F, $\Phi = 0.75$, and $P_{back} = 0$ psig. Across the shortened run time, 20 iterations are performed offering calculated values of 6410 Hz and 1488 m/s for ion probe frequency and individual wave speed, respectively. These calculations were performed at an average iteration time of 0.27 s and feedback frequency of 3.71 Hz. While improvement of iteration speeds is necessary moving forward, these results show the useful application of the proposed method on shorter runs more common throughout the RDE community, even considering the preliminary state of the method.

In every example of diagnostic output, an initial error of wave classification is present during the first 2 s, or more generally during startup because detonation waves are more sporadic and more difficult to image during startup as the system attempts to stabilize. Because this method is developed as a tool to accompany technology maturation as well as offer a potential means of active control in the experimental setting, startup conditions are of less interest than the ability to monitor steady conditions.

The quality of ion probe measurements has expected effects on diagnostic outputs. Clarity of the signal can be impacted by backpressure, port location, probe condition, and other factors. Results to this point have been generated using ion probe data from a port located 2.5 cm downstream of the injector and the anticipated detonation plane. Those results also reflect runs with no initial backpressure. Diagnostic outputs for a run utilizing an ion probe located 5 cm from the injector are plotted in Fig. 19. Operating conditions for this three-wave run are $T_{air} = 400$ °F, $\Phi = 0.6$, and $P_{back} = 0$ psig.

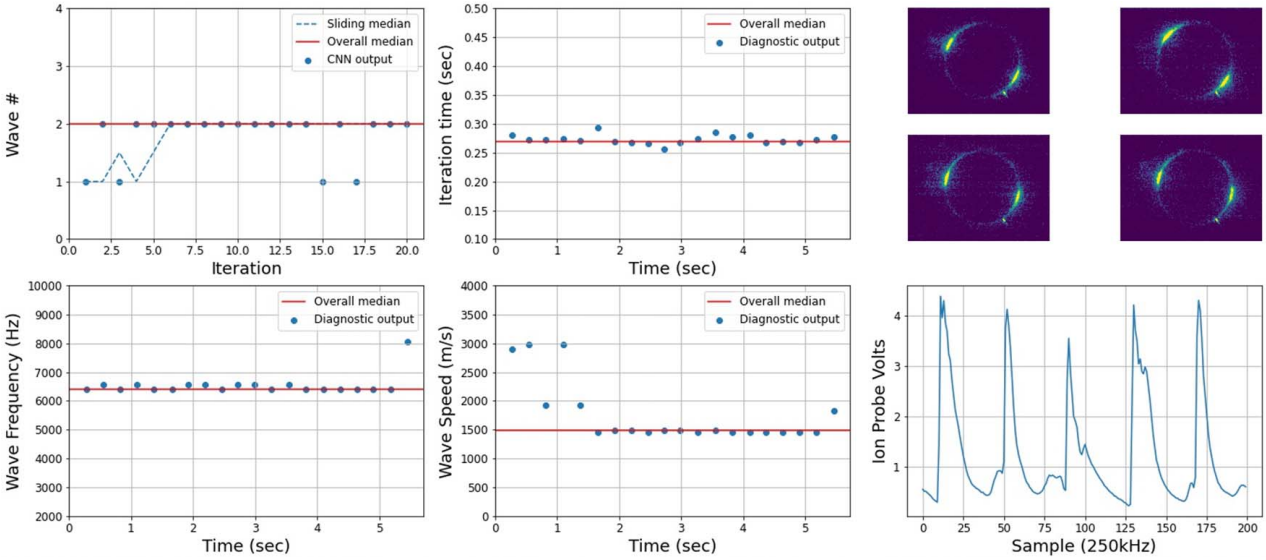

Fig. 18 Diagnostic output monitoring 2 CCW steady waves across short run of with operating conditions: $T_{air} = 320$ °F, $\Phi = 0.75$, $P_{back} = 0$ psig

The ion probe signal is visibly noisy, and the passing of wave fronts is less distinct. Therefore, as seen in the wave frequency plot, auto-correlation inherits a visible degree of uncertainty. Unlike the previous subplots, Fig. 19 includes a spectrogram of recorded pressure, with transducer in an infinite tube pressure (ITP) configuration, in place of iteration time enabling the comparison at a similarly located port and the output of the diagnostic. Like the current method, the spectrogram detects frequencies around 8 kHz and 4 kHz.

It can be seen that although the diagnostic frequency output shows more dispersion than the previous results, a similar behavior of deviation and secondary frequency can be seen in the spectrogram. Still yet, the auto-correlation of the downstream probe doesn't properly distinguish primary and secondary frequencies resulting in the underestimation of frequency and subsequent calculations of uncharacteristically low wave speeds. For this reason, further use, and development of an RDE diagnostic should use data recorded at optimal locations to cleanly define the detonation wave in the absence of more computationally expensive time series data analysis.

Although the results in Fig. 19 are presented to highlight the impact of ion data quality, the image quality remains satisfactory. Four images from the run are shown in the subplot and show a distinct 3 CW wave mode with little pixel intensity outside of detonation wave profiles, offering contrast surpassing that of previous images. In fact, only four misclassifications occur after startup, all of which are negated by the sliding window median. The effects of image quality should be similarly considered with respect to classification accuracy.

Similar to ion probe signals, image quality may be affected by backpressure, preheat temperature, filtering, and camera and intensifier settings. Two examples of poor image quality and the resulting classifications are shown in Figs. 20 and 21.

Because these examples serve to specifically demonstrate the effects of image quality, the full diagnostic outputs are not shown. Figure 20 specifically shows unfocused images where two

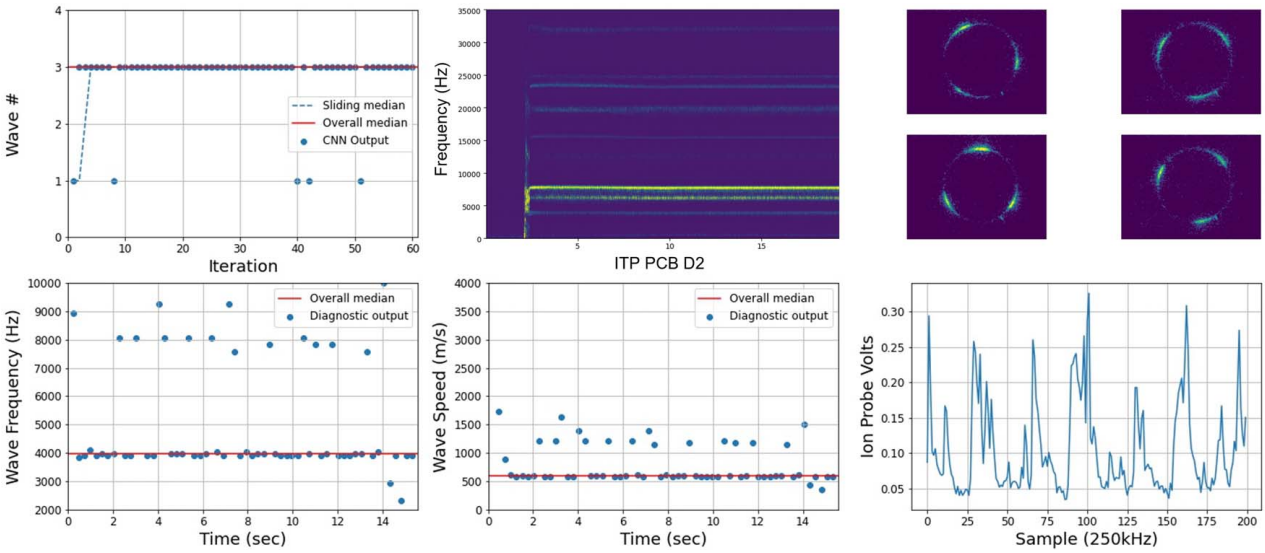

Fig. 19 Diagnostic output monitoring 3 CW steady waves with down-axis ion data at operating conditions: $T_{air} = 400$ °F, $\Phi = 0.6$, $P_{back} = 0$ psig

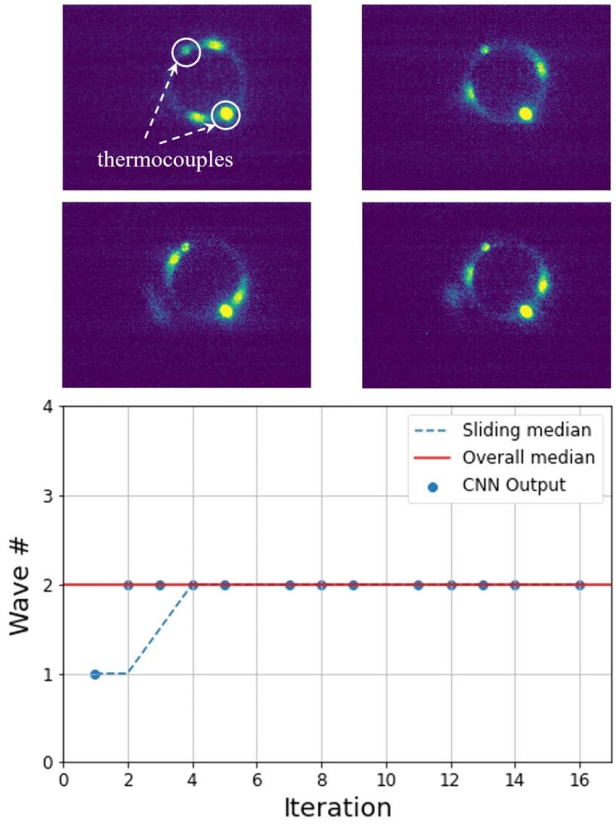

Fig. 20 Diagnostic output monitoring two steady waves with visible thermocouples at operating conditions: $T_{air} = 295$ °F, $\Phi = 0.77$, $P_{back} = 0$ psig

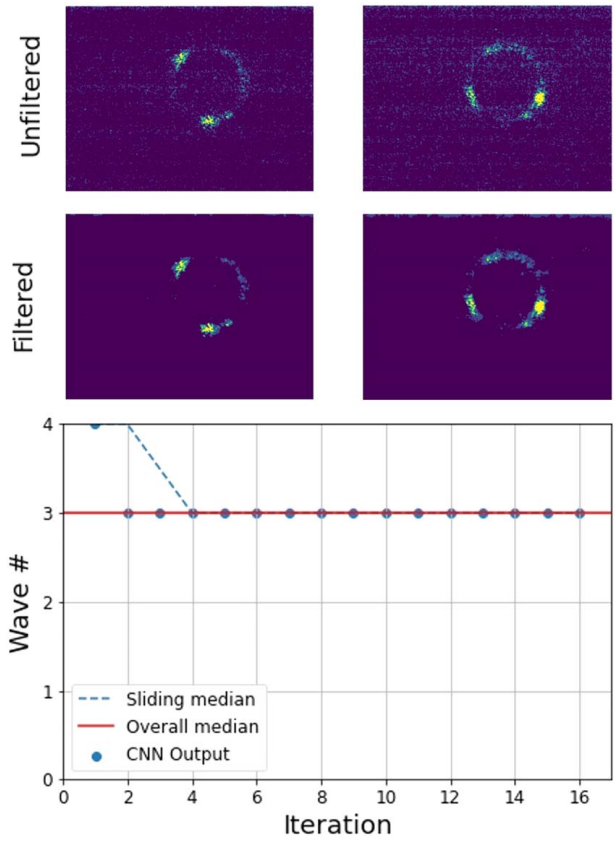

Fig. 21 Diagnostic output monitoring three steady waves with images affected by backpressure at operating conditions: $T_{air} = 345$ °F, $\Phi = 0.45$, $P_{back} = 15$ psig

thermocouples, circled and labeled in first image, consistently appear across all iterations. Without further digital filtering or masking to remove the thermocouples, the CNN classification of wave number remains accurate beyond startup, suggesting a higher resilience for image quality compared to ion data.

A second example of lesser image quality is shown in Fig. 21 where a backpressure of 15 psig resulted in significantly reduced pixel intensities. Because the wave mode within these images is more difficult to discern, only two images are shown in the state at which they are fed to the CNN. For the benefit of the reader, further digital filtering was performed on those two images to highlight the three-wave mode present. Again, the CNN is able to classify the number of waves present in the annulus despite a heavily deteriorated image quality. Ultimately, this resilience is due to the presence of similarly poor images within the training image set, which spans a variety of operating conditions including elevated backpressure. Unlike the images shown in Fig. 20, which are out of focus and experience interference from system thermocouples, images in Fig. 21 do fall within the RDE's operational domain. In addition to the implications of image quality, Fig. 21 also benchmarks an additional set of operating conditions, $T_{air} = 345$ °F, $\Phi = 0.45$, and $P_{back} = 15$ psig at which the diagnostic adequately performs.

No significant signs of under- or over-fitting are observed when the CNN is applied to testing images. Under-fitting would have presented as poor training accuracies in the previous work and did not [13], while over-fitting would result in poor testing accuracy in the current. To further probe over-fitting, the CNN output was evaluated using external images from TU Berlin, provided by Bohon [5,9,30] with varying RDE geometry, framerate, and operating conditions compared to the training set. When this image dissimilarity is introduced, the CNN performs well to properly classify the external images, as shown in Fig. 22, indicating proper generalization.

Across results shown in Figs. 16–22, the testing accuracy varies. For this reason, it is difficult to report a single value representing testing accuracy. Neglecting misclassifications at startup, some cases show close to 100% testing accuracy while others display testing accuracies below 70%. Factors contributing to lesser testing accuracies, including image dissimilarity, are demonstrated in Figs. 20 and 21. In each diagnostic output shown in Figs. 16–22, the sliding median sufficiently dampens the effects of varying testing accuracy on the total diagnostic.

In each presented case, iteration times showed averages around 0.25 s. Of that time, data acquisition accounts for 0.2075 s while classification and calculation only account for 0.0425 s. Storing

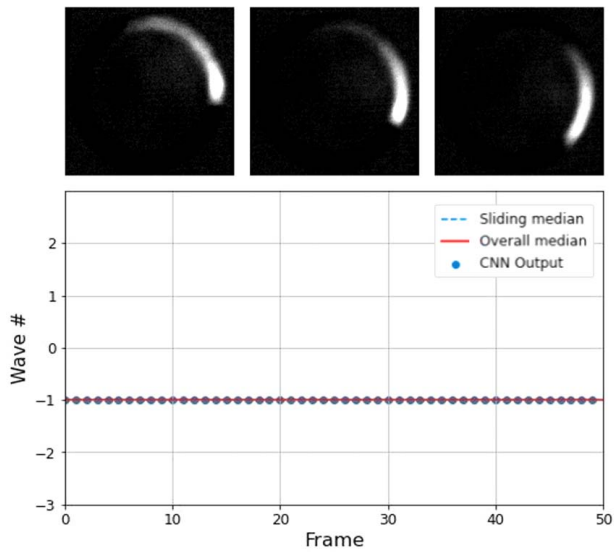

Fig. 22 CNN output monitoring steady detonation waves within images provided by TU Berlin

all outputs of the diagnostic as well as data used to monitor the diagnostic accounts for a significant portion of overall calculation time. To reduce this time and further improve the diagnostic, the volume of saved data beyond raw images and ion probe data can be reduced or completely eliminated. However, classification and calculation time accounts for approximately 20% of total iteration time, meaning sample window times and data acquisition requires 80% of the current diagnostic time. This implies that major improvements to total iteration time may be more attainable through improved experimental setup as opposed to methodology alterations. Therefore, additional options to increase diagnostic speeds by reducing acquisition time, including reduction of image size, shortened time series windows, and improved hardware should be considered. Each of these means of improvement will be considered as future work. Additional future work includes the training of a new CNN with images covering a broader range of wave modes recently observed in the NETL RDE, as well as system integration enabling automatic diagnostic initialization.

While a feedback rate of 4 Hz reported throughout the current study may be a broad timescale compared to the timescale of detonation, it is comparable to expected control timescale factors, namely pneumatic fuel valve responses and control feedback loops within the current laboratory. The impact of this work lies in the ability to analyze detonation wave presence and behavior during RDE operation. Speed and accuracy are both crucial factors of the diagnostic. Speed of calculation and real-time access to experimental data have historically been the primary factors limiting image analysis to post-processing. Speed improvements, offered by the low data volumes required by the posed methodology, lead to a novel real-time capability. It is difficult to adequately benchmark the speed of the methodology since there are no other real-time results in the literature known to the authors at this time. However, total classification and calculation speed can be compared to the well-known detonation surface method [8], which is strictly a post-processing technique. Using 100 images to generate a detonation surface in post-processing, a comparable output which includes wave mode and wave velocities is produced at 0.017 Hz. It should be noted that this method is not specifically optimized for processing speeds but offers an incredibly robust method of image analysis. This comparison of speeds, being 4 Hz for the current method including live data acquisition, and 0.017 Hz for the detonation surface method applied to images in post-processing, serves only to highlight the means by which CNN usage accelerates image analysis to a rate which enables real-time diagnostic loops in practice.

A second diagnostic using a newly trained TSC network [15] will also be deployed in the lab environment and compared to the results of the current method. Eventually, the output of the superior diagnostic should be used to achieve active control of equivalence ratio for a preferred wave mode or wave speed.

At this time, a preferred wave mode or wave speed based on RDE operating conditions is not abundantly clear. However, development of diagnostics and control schemes will inevitably be necessary. It is believed that the speeds of machine learning techniques will be a necessary component of data processing nearing a time scale comparable to what will be required by eventual RDE industrial integration.

Conclusion

Increased operation times in facilities equipped with cooling strategies, such as the water-cooled rig used in this study, facilitate the development of highly efficient detonation characterization techniques which may be optimized for real-time detonation wave monitoring. A real-time RDE diagnostic was developed utilizing a CNN developed to classify wave modes from individual down-axis images and a correlation technique applied to an ionization current, or ion probe data. Live image collection was performed using a common area-scan camera operating at very low-speeds relative to conventional RDE high-speed imaging, paired with an intensifier, and live ion probe data were acquired via an NI cDAQ chassis. Data acquisition within the PYTHON diagnostic environment relied on Pylon and PyDAQmx PYTHON libraries. The diagnostic code was integrated and deployed in the RDE lab environment for use during live runs.

The total diagnostic, including observed accuracy and speed, is unique to this study and text. It is considered to be a first demonstration of real-time monitoring within the RDE community which offers modal certainty, here provided by image classification. The goal of the current work was to demonstrate an altered experimental setup and new methodology to monitor the RDE at feedback rates comparable to expected control feedback loops. The speed of the CNN component, developed in a previous study [13] compared to other image processing techniques is certainly required to achieve this goal. However, the speed of particular interest is not that of the CNN but is that of a total diagnostic which has never before reached speeds necessary to achieve real-time monitoring. These newly observed speeds at which wave mode, wave frequency, and individual wave velocity are obtained prove vital to real-time RDE monitoring capabilities. Without real-time monitoring, active control remains impossible. For this reason, the novel results demonstrated are thought to offer a substantial step toward intelligently controlling an RDE.

Across a variety of operating conditions and wave modes, the developed method was evaluated and found to offer beneficial outputs as a result of combining the spatial certainty of down-axis images, classification speeds of the CNN, and high-quality ion probe measurements. Although the current study utilized ion probe data, the proposed method could be employed with other point measurement time series data, such as ITP pressure transducer data. However, any reduction in data quality or clarity of wavefronts drastically reduce the accuracy of the correlation technique, as was shown in the previous section. Poor image quality showed lesser impact than that of ion data affected by port locations. Sporadic misclassifications of wave mode were mostly bypassed by a sliding window median used to inform later calculations. Reported diagnostic feedback rates around 3–4 Hz exceed existing methods with comparable mode certainty. Approximately 80% of iteration times were attributed to data acquisition, implying significant feedback improvements may be accomplished by hardware alterations or upgrades, which will be considered within future work. The presented method achieves live RDE monitoring in the laboratory environment independent of post-processing, which is believed to be a crucial step toward intelligent RDE active control. This new capability will contribute to future RDE maturation studies of turbine integration and serves as a new milestone of machine learning and computer vision techniques applied to RDE technology.

Acknowledgment

This work was performed in support of the U.S. Department of Energy's Fossil Energy and Carbon Management's Hydrogen with Carbon Management Technologies Program and executed through the National Energy Technology Laboratory (NETL) Research & Innovation Center's Turbines Program. This work would not have been possible without the significant design and operational support provided by Todd Sidwell, Jeffrey Riley, and Richard Eddy.

Disclaimer

This project was funded by the U.S. Department of Energy, National Energy Technology Laboratory, in part, through a site support contract. Neither the United States Government nor any agency thereof, nor any of their employees, nor the support contractor, nor any of their employees, makes any warranty, express or implied, or assumes any legal liability or responsibility for the accuracy, completeness, or usefulness of any information,

apparatus, product, or process disclosed, or represents that its use would not infringe privately owned rights. Reference herein to any specific commercial product, process, or service by trade name, trademark, manufacturer, or otherwise does not necessarily constitute or imply its endorsement, recommendation, or favoring by the United States Government or any agency thereof. The views and opinions of authors expressed herein do not necessarily state or reflect those of the United States Government or any agency thereof.

Conflict of Interest

There are no conflicts of interest.

Data Availability Statement

The datasets generated and supporting the findings of this article are obtainable from the corresponding author upon reasonable request.

Nomenclature

i = iteration count
d_{nom} = nominal RDE diameter
f_{ion} = ion probe frequency
m_{CNN} = CNN wave number classification
t_i = time at increment i
$A_{3.1}$ = air injector area
$A_{3.2}$ = combustor channel area
A_8 = nozzle exit area
P_{back} = backpressure
T_{air} = preheat air temperature
U_w = individual wave speed
Δt_{Ci} = calculation time duration
ΔT_{Si} = sample window time length
τ = sample lag
Φ = equivalence ratio
CCW = counterclockwise
CNN = convolutional neural network
CJ = Chapman–Jouguet
CR = counter-rotating
CW = clockwise
FFT = fast Fourier transform
fps = frames per second
HT = Hough transform
ITP = infinite tube pressure
LECTR = Low Emission Combustor Test and Research Facility
NETL = National Energy Technology Laboratories
PGC = pressure gain combustion
RDE = rotating detonation engine
SR = sampling rate
TRL = technology readiness level
TSC = time series classification

References

[1] Nordeen, C., Schwer, D., Schauer, F., Hoke, J., Cetegen, B., and Barber, T., 2011, "Thermodynamic Modeling of a Rotating Detonation Engine," 49th AIAA Aerospace Sciences Meeting, Orlando, FL, Jan. 4–7.
[2] Johnson, K., Ferguson, D., and Nix, A., 2020, "Validation of Cross-Correlation Detonation Wave Mode Identification Through High-Speed Image Analysis," AIAA SciTech 2020 Forum, Orlando, FL, Jan. 6–10.
[3] Bluemner, R., Bohon, M. D., Paschereit, C. O., and Gutmark, E. J., 2018, "Dynamics of Counter-Rotating Wave Modes in an RDC," 2018 Joint Propulsion Conference, Cincinnati, OH, July 9–11.
[4] Bluemner, R., Bohon, M. D., Paschereit, C. O., and Gutmark, E. J., 2018, "Single and Counter-Rotating Wave Modes in an RDC," 2018 AIAA Aerospace Sciences Meeting, Kissimmee, FL, Jan. 8–12.
[5] Bohon, M. D., Bluemner, R., Paschereit, C. O., and Gutmark, E. J., 2018, "Cross-Correlation as a Tool for Measuring RDC Wave Speed, Direction, and Complexity," 2018 Joint Propulsion Conference, Cincinnati, OH, July 9–11.
[6] Zahn, A., Knight, E., Anand, V., Jodele, J., and Gutmark, E. J., 2018, "Examination of Counter-Rotating Detonation Waves Using Cross-Correlation," 2018 Joint Propulsion Conference, Cincinnati, OH, July 9–11.
[7] George, A. C. S., Kumar, V. A., Driscoll, R. D., and Gutmark, E. J., 2016, "A Correlation-Based Method to Quantify the Operating State in a Rotating Detonation Combustor," 54th AIAA Aerospace Sciences Meeting, San Diego, CA, Jan. 4–8.
[8] Bennewitz, J. W., Bigler, B. R., Hargus, W. A., Danczyk, S. A., and Smith, R. D., 2018, "Characterization of Detonation Wave Propagation in a Rotating Detonation Rocket Engine Using Direct High-Speed Imaging," 2018 Joint Propulsion Conference, Cincinnati, OH, July 9–11.
[9] Bohon, M. D., Bluemner, R., Paschereit, C. O., and Gutmark, E. J., 2019, "High-Speed Imaging of Wave Modes in an RDC," Exp. Therm. Fluid. Sci., **102**, pp. 28–37.
[10] Athmanathan, V., Ayers, Z., Fisher, J., Braun, J., Andreoli, V., Cuadrado, D. G., Fugger, C. A., et al., 2020, "High Speed Imaging of Injection Backflow and Recovery in a Turbine-Integrated High-Pressure Optical RDE (THOR)," AIAA SciTech 2020 Forum, Orlando, FL, Jan. 6–10.
[11] Chacon, F., and Gamba, M., 2019, "Study of Parasitic Combustion in an Optically Accessible Continuous Wave Rotating Detonation Engine," AIAA SciTech 2019 Forum, San Diego, CA, Jan. 7–11.
[12] Athmanathan, V., Fisher, J. M., Ayers, Z., Cuadrado, D. G., Andreoli, V., Braun, J., Meyer, T., Paniagua, G., Fugger, C. A., and Roy, S., 2019, "Turbine-Integrated High-Pressure Optical RDE (THOR) for Injection and Detonation Dynamics Assessment," AIAA Propulsion and Energy 2019 Forum, Indianapolis, IN, Aug. 12–22.
[13] Johnson, K. B., Ferguson, D. H., Tempke, R. S., and Nix, A. C., 2021, "Application of a Convolutional Neural Network for Wave Mode Identification in a Rotating Detonation Combustor Using High-Speed Imaging," ASME J. Therm. Sci. Eng. Appl., **13**(6), p. 061021.
[14] Johnson, K., Ferguson, D. H., and Nix, A. C., 2020, "Individual Wave Detection and Tracking Within a Rotating Detonation Engine Through Computer Vision Object Detection Applied to High-Speed Images," AIAA SciTech 2020 Forum, Orlando, FL, Jan. 6–10.
[15] Johnson, K. B., Ferguson, D. H., and Nix, A. C., 2022, "Time Series Classification Within a Rotating Detonation Engine Through Deep Convolutional Neural Networks Applied to High-Speed Pressure and Ion Probe Data," AIAA SciTech 2022 Forum, San Diego, CA, Jan. 3–7.
[16] Santos-Victor, J. A., Costeira, J. P., Tomé, J. A. B., and Sentieiro, J. J. S., 1993, "A Computer Vision System for the Characterization and Classification of Flames in Glass Furnaces," IEEE Trans. Ind. Appl., **29**(3), pp. 470–78.
[17] Grogan, K. P., and Ihme, M., 2018, "Identification of Governing Physical Processes of Irregular Combustion Through Machine Learning," Shock Waves, **28**(5), pp. 941–54.
[18] Barwey, S., Prakash, S., Hassanaly, M., and Ramen, V., 2021, "Data-Driven Classification and Modeling of Combustion Regimes in Detonation Waves," Flow Turbul. Combust., **106**(4), pp. 1065–89.
[19] Rezzag, T., Burke, R., and Ahmed, K., 2021, "A Kinematic Study of Individual Rotating Detonation Engine Waves Using K-Means Algorithm," ASME Turbo Expo 2021: Turbomachinery Technical Conference and Exposition, Virtual, June 7–11.
[20] Iandola, F. N., Han, S., Moskewicz, M. W., Ashraf, K., Dally, W. J., and Keutzer, K., 2017, "SqueezeNet: AlexNet-Level Accuracy With 50x Fewer Parameters and <0.5MB Model Size," pp. 1–13. arXiv:1602.07360.
[21] Redmon, J., Divvala, S., Girshick, R., and Farhadi, A., 2016, "You Only Look Once: Unified, Real-Time Object Detection," Proceedings of the IEEE Computer Society Conference on Computer Vision and Pattern Recognition, Las Vegas, NV, June 27–30.
[22] Forestier, G., Weber, J., Idoumghar, L., and Muller, P. A., 2019, "Deep Learning for Time Series Classification: A Review," Data Min. Knowl. Discov., **33**(4), pp. 917–963.
[23] Lines, J., Taylor, S., and Bagnall, A., 2018, "Time Series Classification With HIVE-COTE," ACM Trans. Knowl. Discov. Data, **12**(5), pp. 1–35.
[24] Wang, Z., Yan, W., and Oates, T., 2017, "Time Series Classification From Scratch With Deep Neural Networks: A Strong Baseline," Proceedings of the International Joint Conference on Neural Networks, Anchorage, AK, May 14–19.
[25] Görner, M., 2020, "Modern Convnets, SqueezeNet, With Keras and TPUs," https://codelabs.developers.google.com/codelabs/keras-flowers-squeezenet/#0, Accessed March 3, 2020.
[26] Brophy, C. M., and Codoni, J., 2019, "Experimental Performance Characterization of an RDE Using Equivalent Available Pressure," AIAA Propulsion and Energy 2019 Forum, Indianapolis, IN, Aug. 19–22.
[27] "PyPylon: Python Wrapper for the Basler Pylon Camera Software Suite" 2022, https://github.com/basler/pypylon
[28] Cladé, P., 2010, "PyDAQmx: A Python Interface to the National Instruments DAQmx Driver," https://pythonhosted.org/PyDAQmx/
[29] Zahn, A., Knight, E., Anand, V., Jodele, J., and Gutmark, E. J., 2018, "Examination of Counter-Rotating Detonation Waves Using Cross-Correlation," 2018 Joint Propulsion Conference, Cincinnati, OH, July 9–11.
[30] Bohon, M., Bluemner, R., Paschereit, P. O., and Gutmark, E. J., 2018, "Cross-Correlation as a Tool for Measuring RDC Wave Speed, Direction, and Complexity," 2018 Joint Propulsion Conference, Cincinnati, OH, July 9–11.
[31] Chapman, D. L., 1899, "On the Rate of Explosion in Gases," Lond. Edinb. Dublin Philos. Mag. J. Sci., **47**(284), pp. 90–104.